
[View Journal Online](#)
[View Article Online](#)

X-ray diffraction and Density Functional Theory based structural analyses of 2-phenyl-4-(prop-2-yn-1-yl)-1,2,4-triazolone

Shilpa Mallappa Somagond ¹, Ahmedraza Mavazzan ¹, Suresh Fakkirappa Madar ¹,
 Madivalagouda Sannaikar ², Shankar Madan Kumar ³, Sanjeev Ramchandra Inamdar ²,
 Aravind Raviraj Nesaragi ¹, Jagadeesh Prasad Dasappa ⁴ and Ravindra Ramappa Kamble ^{1,*}

¹ Department of Chemistry, Karnatak University, Dharwad, 580003, India

shilpasomagond@gmail.com (S.M.S.), ahmedrazamavazzan804@gmail.com (A.A.M.), surifm444@gmail.com (S.F.M.), nesaragi-aravind@gmail.com (A.R.N.), kamchem9@gmail.com (R.R.K.)

² Department of Physics, Karnatak University, Dharwad, 580003, India

subramanyaphy@gmail.com (M.S.S.), him_lax3@yahoo.com (S.R.I.)

³ Department of Chemistry and Molecular Biology, University of Gothenburg, Gothenburg, 9C 41390, Sweden

madan.mx@gmail.com (S.M.K.)

⁴ Department of Materials Science, Mangalore University, Mangalagangothri, 574199, India

jprasad2003@gmail.com (D.J.P.)

* Corresponding author at: Department of Chemistry, Karnatak University, Dharwad, 580003, India.

e-mail: ravichem@kud.ac.in (R.R. Kamble).

RESEARCH ARTICLE



doi: 10.5155/eurjchem.12.4.459-468.2160

Received: 26 July 2021

Received in revised form: 26 August 2021

Accepted: 23 October 2021

Published online: 31 December 2021

Printed: 31 December 2021

KEYWORDS

N-Arylsydnone
 1,2,4-Triazolone
 X-ray diffraction
 Density functional theory
 Hirshfeld surface analysis
 Molecular electrostatic potential map

ABSTRACT

This study is composed of X-ray diffraction and Density Functional Theory (DFT) based molecular structural analyses of 2-phenyl-4-(prop-2-yn-1-yl)-2,4-dihydro-3H-1,2,4-triazol-3-one (2PPT). Crystal data for C₁₁H₉N₃O: Monoclinic, space group P2₁/c (no. 14), a = 7.8975(2) Å, b = 11.6546(4) Å, c = 11.0648(3) Å, β = 105.212(2)°, V = 982.74(5) Å³, Z = 4, T = 296.15 K, μ(MoKα) = 0.091 mm⁻¹, D_{calc} = 1.346 g/cm³, 13460 reflections measured (5.174° ≤ 2θ ≤ 64.72°), 3477 unique (R_{int} = 0.0314, R_{sigma} = 0.0298) which were used in all calculations. The final R₁ was 0.0470 (I > 2σ(I)) and wR₂ was 0.1368 (all data). The experimentally determined data was supported by theoretically optimized calculations processed with the help of Hartree-Fock (HF) technique and Density Functional Theory with the 6-311G(d,p) basis set in the ground state. Geometrical parameters (Bond lengths and angles) as well as spectroscopic (FT-IR, ¹H NMR, and ¹³C NMR) properties of 2PPT molecule has been optimized theoretically and compared with the experimentally obtained results. Hirshfeld surface analysis with 2D fingerprinting plots was used to figure out the possible and most significant intermolecular interactions. The electronic characterizations such as molecular electrostatic potential map (MEP) and Frontier molecular orbital (FMO) energies have been studied by DFT/B3LYP approach. The MEP imparted the detailed information regarding electronegative and electropositive regions across the molecule. The HOMO-LUMO energy gap as high as 5.3601 eV was found to be responsible for the high kinetic stability of the 2PPT.

Cite this: *Eur. J. Chem.* 2021, 12(4), 459-468

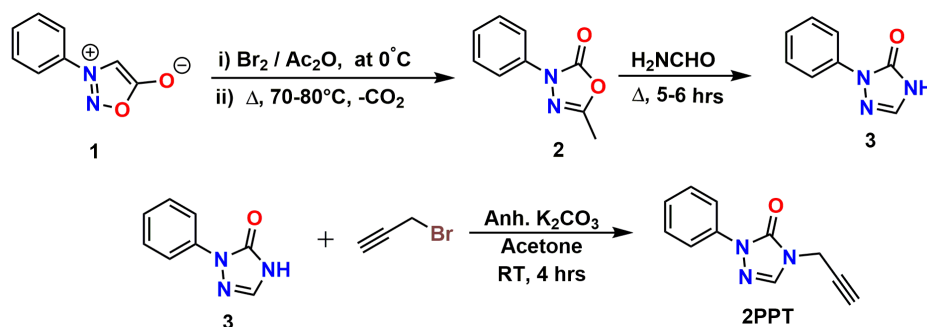
Journal website: www.eurjchem.com

1. Introduction

Organic scaffolds containing 1,2,4-triazole moiety have been investigated for their outstanding activities such as antihypertensive, antiviral, and anticancer, *etc.* and hence, they have established themselves as important pharmacophores [1-5]. In this study, we have synthesized a 1,2,4-triazole containing molecule linked with ethynyl end (2PPT), which is a possible synthon for carrying out interesting cycloaddition reactions [6-9].

Single-crystal X-ray crystallography (XRD) remains the most important approach for generating the high-resolution 3D structural information for small as well as biomacromolecules, independent of their size. It is a non-destructive analytical tool that can afford comprehensive data regarding the internal

crystal-lattice of a crystalline matter. It can decipher critical crystal related information, *viz.*, unit cell dimensions, bond lengths, bond angles and site-ordering, *etc.* In recent days, the physical features of pharmacologically important organic molecules can be predicted by various advanced computational techniques [10,11]. For example, density functional theory is a quantum-mechanical method used to calculate the electronic structure of atoms, molecules and solids in chemistry and physics. Density Functional Theory (DFT) has succeeded to grab the attention of the researchers all over the world for theoretical modelling. It has a broad spectrum of applications in chemical and material sciences for the interpretation and prediction of molecular geometry, spectroscopic and other characteristic molecular properties and thereby accompanying the experimental results.



Scheme 1

Nobel Prize for the development of DFT in the year 1998 evidences its enormous importance in both the physics and chemistry [12-14].

We had earlier reported the synthesis of 2-(4-methoxy phenyl)-4-[[2'-(1*H*-tetrazol-5-yl)biphenyl-4-yl]methyl]-2, 4-dihydro-3*H*-1, 2, 4-triazol-3-one and the XRD, Hirshfeld surface analyses and corroborated the same with the help of DFT studies [15]. In the present study, X-ray diffraction analysis of the 2-phenyl-4-(prop-2-yn-1-yl)-2,4-dihydro-3*H*-1,2,4-triazol-3-one (2PPT) in order to obtain crystal structure as well as geometrical parameters is reported. Further, XRD analysis found beneficial in determining the intermolecular and intramolecular hydrogen bonding in 2PPT. In addition, the synthesized 2PPT molecule was well characterized by FT-IR, ¹H and ¹³C NMR spectroscopic techniques. This is an interesting molecule since it is a potential starting material for click chemistry [10-14]. There is a presence of C≡C-H group in this molecule 2PPT and this proton is present in the shielded region in the anisotropic magnetic field created by triple bond. Therefore, the chemical shift values for this proton will be lower (Up field shift). The analysis of experimental as well as theoretical chemical shift (δ) values will be interesting for such novel molecules. In this way, the experimental chemical shift values of this proton (¹H NMR), and that of C≡C (¹³C NMR) can be compared with the theoretical chemical shift values obtained from DFT studies. In order to explain hydrogen bonding, chemical reactivity, dipole moment, detection of partial positive, and negative charges over the atoms, and electronegativity, molecular electrostatic potential map is believed to be very salutary. This MEP mapping was carried out for the title compound 2PPT applying DFT studies.

2. Experimental

2.1. Materials

The starting materials and solvents used in the present work have been purchased commercially. The reactions according to Scheme 1 [4,5] were monitored by TLC plates procured from Sigma-Aldrich. Melting point of the title compound 2PPT has been recorded on electric melting point apparatus and uncorrected. The FT-IR spectra (KBr) were recorded in the region 4000-500 cm⁻¹ on a Nicolet 170 SX FT-IR spectrometer. ¹H NMR (400 MHz) and ¹³C NMR (100 MHz) spectra were recorded by Jeol-FT-NMR spectrometer using DMSO-*d*₆ as solvent and tetramethylsilane (TMS) as an internal reference. Mass spectrometry was carried out using LC/MS (Synapt G2 HDMS ACQUITY UPLC).

2.2. Synthesis

2.2.1. Synthesis of 3-(phenyl)-5-methyl-1,3,4-oxadiazol-2(3*H*)-one (2)

A round bottom flask was charged with *N*-phenylsydnone (1, 0.010 mol) in acetic anhydride (5.00 mL) to which bromine (0.011 mol) in acetic anhydride (5.00 mL) was added drop-wise with constant stirring for 45 min at 0-5 °C. After the addition was completed, the solution was heated on water bath at 70-80 °C until the evolution of CO₂ ceased. The solution was quenched with crushed ice to get the crude product after attaining room temperature [16]. The crude product 2 obtained was filtered and washed with hexane.

2.2.2. Synthesis of 2-phenyl-2*H*-1,2,4-triazol-3(4*H*)-one (3)

The compound 2 (0.010 mol) in formamide (10.00 mL) was refluxed for 5-6 hours. Completion of the reaction was monitored by TLC. After the completion, the solution was poured into ice cold water to get crude product 3. The crude product obtained was recrystallized from ethanol to get yellow crystals of compound 3 [16].

2.2.3. Synthesis of 2-phenyl-4-(prop-2-ynyl)-2*H*-1,2,4-triazol-3(4*H*)-one (2PPT)

A mixture of 2-aryl-2*H*-1,2,4-triazol-3(4*H*)-one 3 (0.020 mol), anhydrous K₂CO₃ (0.025 mol) and 3-bromoprop-1-yne (0.020 mol) in dry acetone (20 mL) was stirred at room temperature for 4 hrs. After completion of the reaction, the solvent was removed under reduced pressure to get the colorless crystals of compound 2PPT was filtered. FT-IR (KBr, ν , cm⁻¹): 3295 (C-H str.), 3088 (C-H str.), 2973 (C-H str.), 2127 (C≡C str.), 1698 (C=O str.), 1599 (C=N str.), 1567 (C=C str.), 1397 (CH₂ bend.), 978-795 (Ar-H bend.). ¹H NMR (400 MHz, CDCl₃, δ , ppm): 2.495 (t, 1H, CH), 4.477 (d, 2H, CH₂), 7.738 (s, 1H, CH, triazole), 7.929 (d, 2H, Ar-H), 7.413 (t, 2H, Ar-H), 7.217 (t, 1H, Ar-H).

2.3. X-ray data collection and refinement

A single crystal of 2PPT has been grown by slow evaporation method and a crystal (0.21×0.23×0.24 mm) was chosen for XRD analyses and all the measurements were made on Rigaku Saturn 724 diffractometer using graphite monochromated MoK α radiation. The data were collected at 23±1 °C. All calculations were performed using the CrystalClear [17] crystallographic software package and refinement was performed by direct techniques and refined by full-matrix least squares method on F² using SHELXS and SHELXL programs [18]. All non-hydrogen atoms were revealed within the first difference Fourier map itself. Riding model was used to position all the hydrogen atoms geometrically. The Fourier map did not show any chemical significance after ten cycles of refinement. PLATON [19] and MERCURY [20] were used for the execution of geometrical computations and creating molecular packing diagrams, respectively. Table 1 shows the crystal data and structure refinement.

Table 1. Crystal data and structure refinement details for the title compound 2PPT.

| | |
|--|---|
| Empirical formula | C ₁₁ H ₉ N ₃ O |
| Formula weight | 199.21 |
| Temperature (K) | 296.15 |
| Crystal system | Monoclinic |
| Space group | <i>P2₁/c</i> |
| <i>a</i> , (Å) | 7.8975(2) |
| <i>b</i> , (Å) | 11.6546(4) |
| <i>c</i> , (Å) | 11.0648(3) |
| α (°) | 90 |
| β (°) | 105.212(2) |
| γ (°) | 90 |
| Volume (Å ³) | 982.74(5) |
| <i>Z</i> | 4 |
| ρ _{calc} (g/cm ³) | 1.346 |
| μ (mm ⁻¹) | 0.091 |
| F(000) | 416.0 |
| Crystal size (mm ³) | 0.24 × 0.23 × 0.21 |
| Radiation | MoKα (λ = 0.71073) |
| 2θ range for data collection (°) | 5.174 to 64.72 |
| Index ranges | -11 ≤ <i>h</i> ≤ 11, -14 ≤ <i>k</i> ≤ 17, -16 ≤ <i>l</i> ≤ 16 |
| Reflections collected | 13460 |
| Independent reflections | 3477 [R _{int} = 0.0314, R _{sigma} = 0.0298] |
| Data/restraints/parameters | 3477/0/136 |
| Goodness-of-fit on F ² | 1.031 |
| Final R indexes [I ≥ 2σ (I)] | R ₁ = 0.0470, wR ₂ = 0.1213 |
| Final R indexes [all data] | R ₁ = 0.0716, wR ₂ = 0.1368 |
| Largest diff. peak/hole (e.Å ⁻³) | 0.18/-0.21 |

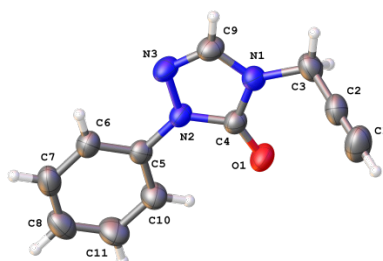
**Figure 1.** Molecular structure of the 2PPT showing the atomic numbering system.

Figure 1 represents the Oak Ridge Thermal-Ellipsoid Plot Program (ORTEP) of the molecule drawn at 50% probability [20].

2.4. Computational methods

All the computations were accomplished on Becke's three parameter hybrid functional using the LYP correlation functional (B3LYP) [21,22]. The vibrational frequencies were scaled down by 0.9679 scaling factor. All computational work was carried out with the help of Gaussian 09 software package. The vibrational wavenumbers, ¹H and ¹³C chemical shifts and frontier molecular orbital energies were determined by means of 6-311G(d,p) basis set [23,24]. Structural optimization of 2PPT was carried out by frequency analysis and the geometry was fully optimized with TMS as internal. The δ values (¹H and ¹³C NMR) in ppm were estimated with the help of GIAO technique for calculating nuclear magnetic shielding tensors, since it is the most accurate method than other approaches for the same sized basis set. In addition, it allows the calculation of the absolute chemical shielding formed as a result of the electronic environment around particular nuclei [25].

2.5. Hirshfeld surface analysis

Intermolecular interactions of the molecule in a crystal structure are studied quantitatively by the Hirshfeld surface analysis, which also gives the insights of the crystal packing. Crystal Explorer 3.1 software is useful in mapping the Hirshfeld surfaces and fingerprint plots [26]. The surface was realized by the normalized contact distance (*d_{norm}*), which was obtained using a high surface resolution with a static color scale of -0.222

(red) to 1.274 Å (blue) and calculated using the Equation (1) as given below.

$$d_{\text{norm}} = \frac{d_i - r_i^{\text{vdw}}}{r_i^{\text{vdw}}} + \frac{d_e - r_e^{\text{vdw}}}{r_e^{\text{vdw}}} \quad (1)$$

where *d_e* = Distance from the Hirshfeld surface to the nearest nucleus outside the surface, *d_i* = Distance to the nearest nucleus inside the surface, and *r^{vdw}* is the van der Waals (vdW) radius of the atom. The *d_{norm}* parameter shows a surface with a red-white blue color scheme. Bright red spots exhibit intermolecular contacts less than their vdW radii, while the blue spots indicate intermolecular contacts longer than their vdW radii. White spots are the sum of their vdW radii. The molecular electrostatic potential is mapped on HS using Slater type orbital simulated by 3 Gaussians basis set at the Hartree-Fock theory. Crystal explorer integrated geometries were used as inputs to the TONTO [27-29].

3. Results and discussion

3.1. Molecular geometry

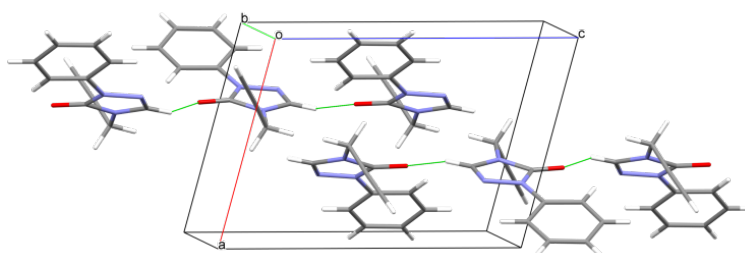
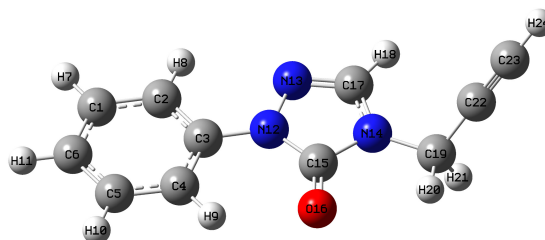
An appraisal of the electronic properties of intermolecular interactions in crystals is an important aspect of quantitative crystal engineering and thus helps in designing novel functional materials. Hence, single crystal X-ray diffraction study is useful in understanding the 3D structural data and the binding stereochemistry. This will help in understanding the mode of binding of small molecules to bio-macromolecules and hence this information can be used to predict how lead molecules will interact with the biological receptors [30].

Table 2. Bond lengths and angles for 2PPT molecule.

| Atom | Atom | Length (Å) | Theoretical (Å) | Atom | Atom | Length (Å) | Theoretical (Å) | | |
|------|------|------------|-----------------|-----------------|------|------------|-----------------|------------|-----------------|
| O1 | C4 | 1.2186(12) | 1.248 | C1 | C2 | 1.1710(19) | 1.204 | | |
| N1 | C3 | 1.4589(14) | 1.466 | C2 | C3 | 1.4590(17) | 1.462 | | |
| N1 | C4 | 1.3783(13) | 1.408 | C5 | C6 | 1.3879(15) | 1.402 | | |
| N1 | C9 | 1.3585(14) | 1.378 | C5 | C10 | 1.3860(15) | 1.402 | | |
| N2 | N3 | 1.3917(12) | 1.415 | C6 | C7 | 1.3846(17) | 1.394 | | |
| N2 | C4 | 1.3738(13) | 1.393 | C7 | C8 | 1.368(2) | 1.398 | | |
| N2 | C5 | 1.4126(13) | 1.423 | C8 | C11 | 1.375(2) | 1.396 | | |
| N3 | C9 | 1.2871(15) | 1.310 | C10 | C11 | 1.3815(17) | 1.397 | | |
| Atom | Atom | Atom | Angle (°) | Theoretical (°) | Atom | Atom | Atom | Angle (°) | Theoretical (°) |
| C4 | N1 | C3 | 123.49(9) | 122.28 | N2 | C4 | N1 | 103.11(8) | 103.03 |
| C9 | N1 | C3 | 128.31(10) | 129.26 | C6 | C5 | N2 | 118.93(9) | 118.97 |
| C9 | N1 | C4 | 108.19(9) | 108.45 | C10 | C5 | N2 | 120.94(9) | 120.54 |
| N3 | N2 | C5 | 119.77(8) | 119.97 | C10 | C5 | C6 | 120.12(10) | 119.49 |
| C4 | N2 | N3 | 111.78(8) | 111.57 | C7 | C6 | C5 | 119.35(11) | 120.63 |
| C4 | N2 | C5 | 127.83(8) | 128.45 | C8 | C7 | C6 | 120.93(12) | 119.37 |
| C9 | N3 | N2 | 104.17(8) | 104.72 | C7 | C8 | C11 | 119.26(12) | 112.22 |
| C1 | C2 | C3 | 177.84(14) | 179.51 | N3 | C9 | N1 | 112.75(9) | 119.11 |
| N1 | C3 | C2 | 112.55(9) | 113.13 | C11 | C10 | C5 | 118.99(11) | 120.91 |
| O1 | C4 | N1 | 127.20(10) | 120.16 | C8 | C11 | C10 | 121.34(12) | 103.03 |
| O1 | C4 | N2 | 129.69(10) | 130.80 | | | | | |

Table 3. Intermolecular and Intramolecular interactions.

| D-H...A | D-H | H...A | D...A | ∠D-H...A | Symmetry |
|--------------------|------|-------|------------|----------|-----------------|
| C(6)-H(6)...N(3) | 0.93 | 2.44 | 2.7794(17) | 101 | - |
| C(10)-H(10)...O(1) | 0.93 | 2.33 | 2.9445(16) | 123 | - |
| C(9)-H(9)...O(1) | 0.93 | 2.35 | 3.0961(16) | 137 | x, 3/2-y, 1/2+z |

**Figure 2.** Packing of the 2PPT molecule.**Figure 3.** Optimized geometry of the 2PPT.

The extracted data from X-ray analysis, collected reflections and other parameters of the final refinement are reported in Table 1. Bond lengths and angles of 2PPT are given in Table 2. The molecular structure of 2PPT is given in Figure 1. The packing diagram of the 2PPT molecule is shown in Figure 2.

Single crystal XRD analysis of 2PPT shows that in the triazolone ring distance N3-C9 (1.2871(15) Å) is smaller than that of N1-C4 (1.3783(13) Å), which in turn signifies the double bond between N3 and C9. Akin bonds N1-C4 and N2-C4 having distances of 1.3783(13) and 1.3738(13) Å, respectively, are single bonds as they are greater than N3-C9 bond. The distance C1-C2 (1.1710(19) Å) is clearly a triple bond.

In the 1,2,4-triazolone ring the sum of the bond angles O1-C4-N1 (127.20(10)°), O1-C4-N2 (129.69(10)°) and N2-C4-N1 (103.11(8)°) is clearly a 360° which confirms the sp^2 hybridization of the C4 carbonyl carbon atom. The slightly deviated bond angle C1-C2-C3 (177.84(14)°) from 180° confirms the presence of a triple bond between C1 and C2.

XRD analysis of 2PPT confirms the presence of intermolecular and intramolecular hydrogen bonding. The 2PPT molecules are linked via C(9)-H(9)...O(1) intermolecular hydrogen bond, which further shows the presence of C(6)-H(6)...N(3) and C(10)-H(10)...O(1) intramolecular hydrogen bonds. Details of these interactions are as shown in Table 3.

In order to support the experimental parameters, the molecular structure of the 2PPT was deployed for theoretical calculations and the molecular geometry was optimized using DFT in ground state (Figure 3). The optimized parameters (Bond lengths and angles) are compared with those of the experimental values (Table 2). However, a very minor difference that occurred between the theoretical and experimental values which is due to the fact that the theoretical results correspond to the isolated gaseous phase and the experimental data is obtained for a molecule in solid phase.

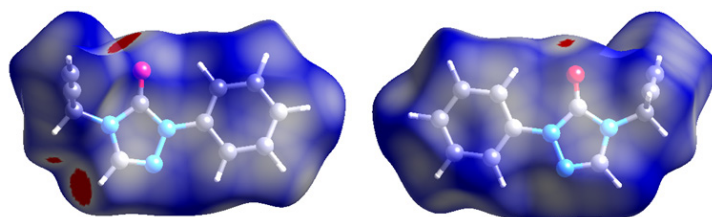


Figure 4. d_{norm} mapped Hirshfeld surface for representing intercontact of 2PPT with different orientations.

3.2. Hirshfeld surface analyses

Intermolecular attractions were ascertained by the Hirshfeld surface computational analysis. Figure 4 represents the d_{norm} mapped Hirshfeld surface using red-blue-white color plot. The red color region with $-d_{norm}$ value corresponds to the closer contacts and the longer contacts represent the blue region with $+d_{norm}$ values, and the $d_{norm} = 0$ indicates the white regions [31-34]. Short interatomic interactions result into dark red spots and the other interactions are shown as light red spots on d_{norm} surfaces. Intercontact with respect to d_i and d_e were plotted with the help of 2D fingerprint plots. The molecule acts as a donor if the molecule shows $d_i < d_e$ and the molecule acts as the acceptor if $d_i > d_e$ [35,36].

Red region exhibits the dominant interactions between O and H as shown in Figure 4. The bifurcated long spikes resulted because of strong H-bonds. The outer spikes are due to the $N \cdots H$ type of interactions and the inner spikes are the result of $O \cdots H$ interactions. The spikes closer to d_e axis illustrate the interaction of the molecule as a donor, whereas the spikes on the opposite end (*ie.*, near d_i axis) illustrates the interactions of the molecule as an acceptor. The little spike in between two extreme bifurcated spike represents H-H type of interactions.

The percentage contributions of various intermolecular contacts to the Hirshfeld surface have been represented in Figure 5. We observed that the maximum contribution to Hirshfeld surface was from H-H interaction which was about 39.8%. This was followed by contributions from C-H, O-H, and N-H which were found to be 29.0, 10.4 and 9.3%, respectively.

3.3. Molecular electrostatic potential map

Molecular electrostatic potential (MEP) is an important concept in molecular modelling calculations as it provides accurate information on the active sites of chemical entities. It is crucial in assessing chemical addition nature by which a chemical structure is most probable to go through. Molecular electrostatic potential maps are the peripheral area of a structure resulted from a group of intersecting spheres, where their centers are aligned with the nucleus of every atom. These spheres are formed from van der Waals radii of the interested atoms. Also, MEP maps explain valuable information about the interaction, active sites as well as resolving the nature of chemical addition, through which a molecule is most probable to undergo whether electrophilic or nucleophilic addition [37-44]. Based upon this idea, molecular modelling was conducted for mapping the molecular electrostatic potential of 2PPT. In this regard, calculations were done using high theoretical DFT level through B3LYP/6-31G(d,p) method.

On the basis of the positive and negative values of the electrostatic potential $V(r)$, we can obtain useful information about electropositive and electronegative sites of the molecule. The MEPS region of the molecule ranges from -6.544 to +6.544 a.u. The red color region around the carbonyl oxygen O_1 of triazolone ring and phenyl ring represents a negative electrostatic potential which shows affinity towards electrophilic moieties, whereas on the flip side the blue color across

the nitrogen atom N_1 and ethynyl end reveals positive electrostatic potential and thereby these sites are more prone for nucleophilic attacks (Figure 6).

3.4. Vibrational spectroscopy

A very useful illustration on the bonding force and the intermolecular bond strength can be obtained by analyzing the vibrational spectroscopy. Hence, by using DFT/B3LYP with 6-311G(d,p) basis set, the theoretical vibrational frequencies of the 2PPT molecule were calculated and compared with the experimentally observed values. The experimental and theoretical IR spectra of 2PPT are given in Figure 7. The molecule has some of the characteristic stretching vibrations in the IR spectrum, they are CO, CH, CC, and CN. The alkyne CH *ie.*, $\equiv C-H$ shows distinctive stretching frequency and is observed experimentally at 3295 cm^{-1} whereas theoretically it is calculated at 3289 cm^{-1} . The stretching vibration of alkyne $C \equiv C$ is experimentally observed at 2127 cm^{-1} while calculated at 2216 cm^{-1} . The band at 2973 cm^{-1} is corresponding to the stretching vibration of CH of methylene protons of 2PPT and the same is theoretically computed at 2989 cm^{-1} . The carbonyl (triazolone ring) of 2PPT shows a sharp strong band at 1698 cm^{-1} and calculated at 1683 cm^{-1} . The bands at 3089 and 1567 cm^{-1} corresponds to stretching vibrations of CH and CC (phenyl ring) of 2PPT, respectively, and were calculated at 3066 and 1572 cm^{-1} . The CN (imine) band of 2PPT was observed experimentally at 1599 cm^{-1} and computed at 1630 cm^{-1} . For 2PPT, methylene CH bending vibrations experimentally observed at 1397 cm^{-1} and calculated at 1399 cm^{-1} . The bending vibrations of aromatic CH observed in $978-797 \text{ cm}^{-1}$ region and are calculated at $982-795 \text{ cm}^{-1}$.

3.5. NMR spectroscopy

NMR spectroscopic technique is of great use in identifying the hydrogen and carbon environment of the organic molecules. The experimental 1H and ^{13}C NMR spectra of 2PPT were recorded in $CDCl_3$ at 400 MHz by using tetramethylsilane (TMS) as internal standard. With the help of DFT (B3LYP) method with 6-311G(d,p) basis set and the theoretical GIAO (Gauge including/invariant atomic orbitals) 1H and ^{13}C chemical shifts were calculated and compared with experimentally obtained results. The positions of atoms are numbered as shown in Figure 8.

In the experimental 1H NMR spectrum of 2PPT, the alkyne proton (C_1-H) was resonated at δ 2.495 ppm. The same proton has been calculated at δ 1.39 ppm for B3LYP methods with the 6-311G(d,p) set. Both the methylene protons ($H-C_3-H$) have resonated at δ 4.477 ppm while the calculated chemical shifts at δ 3.07-3.97 ppm. Azomethine proton of 1,2,4-triazolone ring (C_9-H) of 2PPT observed at δ 7.738 ppm, whereas, the computed chemical shift of corresponding protons has been found at δ 7.94 ppm. Finally, the protons of the phenyl ring of 2PPT resonated at δ 7.199-7.939 ppm, which are calculated at δ 6.10-6.50 ppm (Table 4).

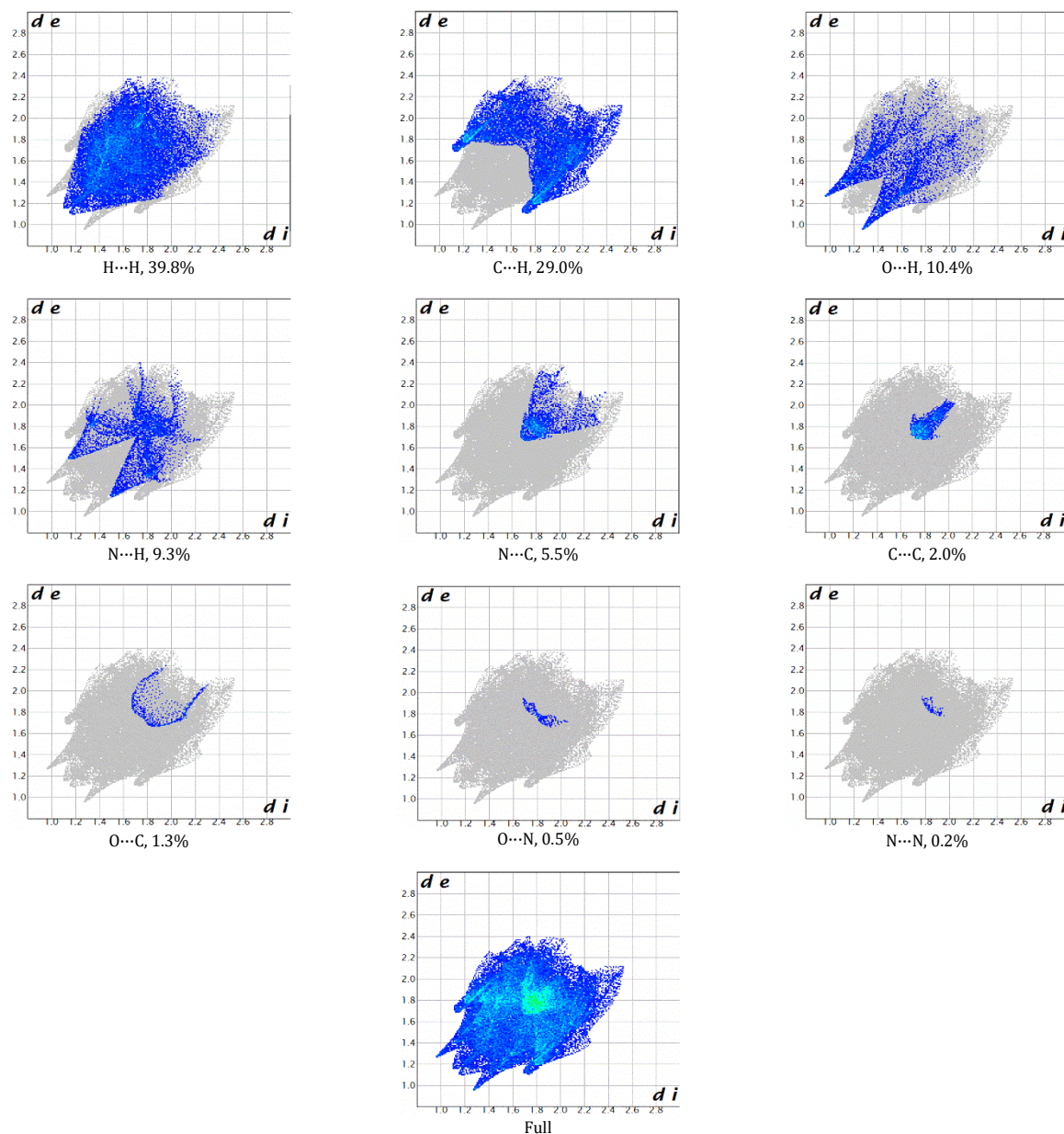


Figure 5. 2D Fingerprint plots of the 2PPT molecule. The contribution to the whole intermolecular interactions can be seen.

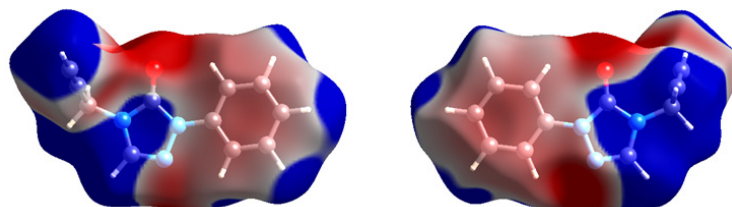


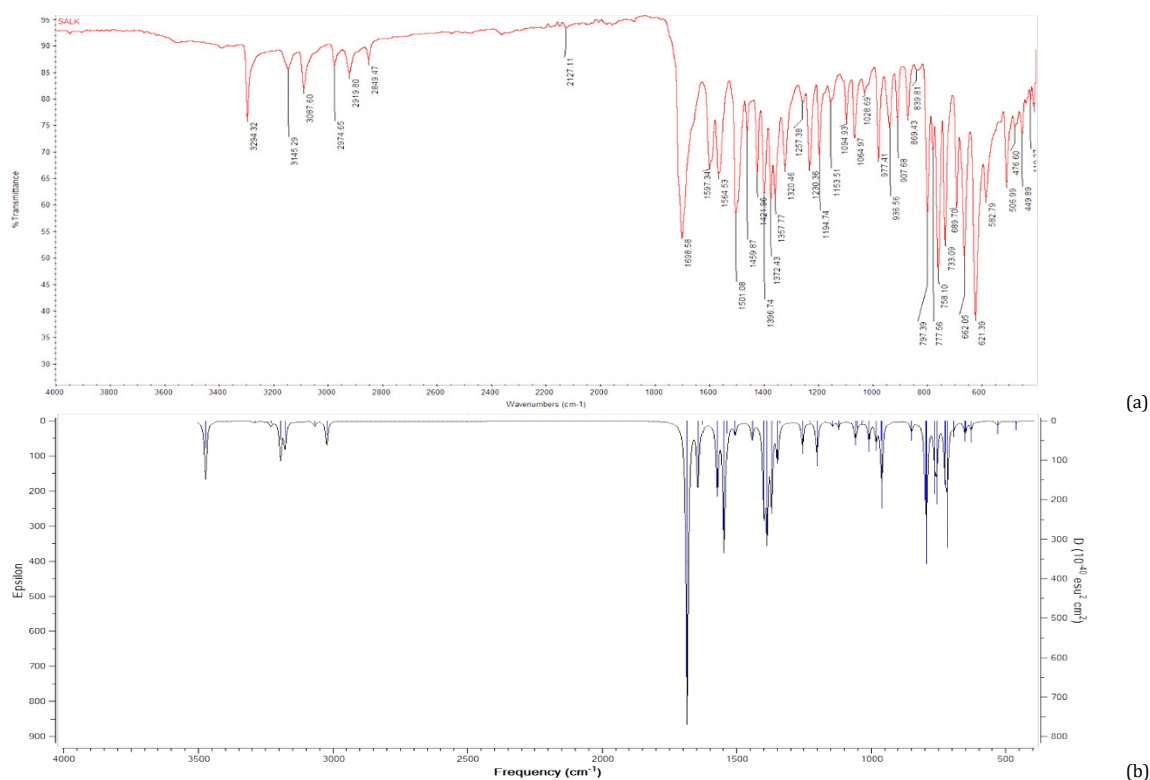
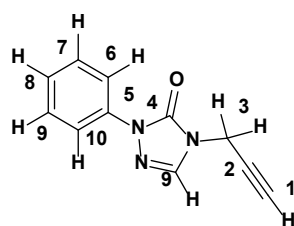
Figure 6. The molecular electrostatic potential surface of 2PPT.

^{13}C NMR spectrum of 2PPT has only one signal in aliphatic region at δ 32.326 ppm due to C_3 . This signal was computed at δ 26.0 ppm for B3LYP level. There are two signals at δ 75.27 and 75.634 ppm for C_1 and C_2 , respectively, in the alkyne region which indicate the presence of C-C triple bond in 2PPT, while these signals were evaluated at δ 73.0 and 76.0 ppm. Chemical shift at δ 150.878 ppm corresponds to C_4 of 2PPT since this carbon is doubly bonded to electro negative and hence appears in the deshielded region, while the same is computed at δ 151.0

ppm. Imine carbon (C_9) of 2PPT resonated at δ 135.021 ppm. while calculated at δ 136.0 ppm. Rests of the signals were observed in the aromatic region. C_5 of the phenyl ring was observed at δ 137.713 ppm which is slightly downfield (as compared to other C atoms of the phenyl ring) because of the direct attachment of electron withdrawing triazolone ring, which is to be calculated at δ 138.0 ppm. Due to chemical and magnetic equivalence, C_6 and C_{10} show single peak at δ 118.809 ppm in experimental spectrum.

Table 4. Experimental and theoretical ^1H and ^{13}C NMR chemical shifts of 2PPT.

| Nucleus | Atoms | Experimental (ppm) | B3LYP/6-311G(d,p) (ppm) |
|-----------------|--|--------------------|-------------------------|
| ^1H | 1H (C ₁ -H) | 2.495 | 1.39 |
| | 2H (C ₃ CH ₂) | 4.477 | 3.01-3.97 |
| | 1H (C ₉ -H) | 7.738 | 7.91 |
| | 2H (C ₆ , C ₁₀ Ar-H) | 7.929 | 6.40-6.50 |
| | 2H (C ₇ , C ₁₁ Ar-H) | 7.413 | 6.18-6.20 |
| | 1H (C ₈ Ar-H) | 7.217 | 6.12 |
| ^{13}C | C ₁ | 75.270 | 73.00 |
| | C ₂ | 75.634 | 76.00 |
| | C ₃ | 32.326 | 26.00 |
| | C ₄ | 150.878 | 151.00 |
| | C ₉ | 135.021 | 136.00 |
| | C ₅ | 137.713 | 138.00 |
| | C ₆ , C ₁₀ | 118.809 | 114.50-116.00 |
| | C ₇ , C ₁₁ | 129.118 | 126.80-127.00 |
| C ₈ | 125.849 | 124.00 | |

**Figure 7.** Experimental (a) and theoretical (b) IR spectra of 2PPT.**Figure 8.** Numbering of carbon atoms in 2PPT.

These are computed at δ 114.5 and 116.0 ppm, respectively, by B3LYP. Similarly, C₇ and C₁₁ resonated experimentally at δ 129.118 ppm and corresponding signals were computed at δ 126.8 and 127.0 ppm, respectively. Finally, C₈ of 2PPT resonated at δ 125.841 ppm while calculated at δ 124.0 ppm.

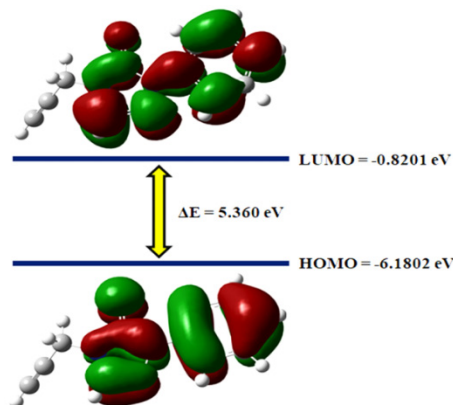
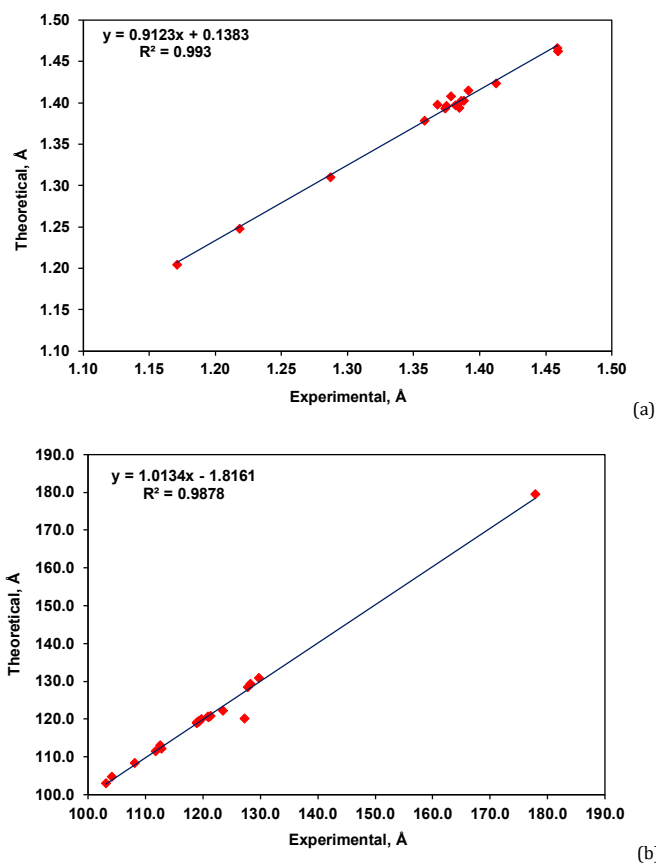
3.6. Frontier molecular orbital analysis

Frontier molecular orbital (FMO) analysis is of great use in determining the electronic and optical properties of the organic

molecule [45,46]. The highest occupied molecular orbital (HOMO) acts as electron donor whereas on the other hand lowest unoccupied molecular orbital (LUMO) acts as electron acceptor. For 2PPT, the energies of HOMO and LUMO are -6.1802 and -0.8201 eV, respectively. The band gap (E_g) is the difference between the energy of LUMO to that of HOMO, which has been important in explaining the reactivity and stability of organic molecules. Lower the E_g of the molecule corresponds to the least stability and more reactivity whereas higher E_g has relevance to most stability and less reactivity.

Table 5. Global reactivity parameters.

| Global reactivity parameter | Value (eV) |
|--|------------|
| Chemical hardness, (η) | 2.68 |
| Electronegativity (χ) | 3.50 |
| Electronic chemical potential (μ) | -3.50 |
| Global electrophilicity index (ω) | 2.285 |
| Chemical softness (s) | 0.186 |

**Figure 9.** The HOMO-LUMO plot of the 2PPT molecule.**Figure 10.** Correlation graphs between the experimental and theoretical (a) bond lengths and (b) bond angles.

For 2PPT, E_g has found to be 5.3601 eV. The large E_g value indicates the high stability of the 2PPT (Figure 9). The global reactivity parameters have been calculated using HOMO and LUMO energies as given in Table 5. The equations for the calculation of these parameters are given in electronic supplementary information.

3.7. Structural correlation of 2PPT by DFT and XRD studies

Conventionally, two methods were used in comparison of the molecular structures. The first method is to calculate the correlation value (R^2). The optimized geometrical parameters (bond lengths and angles) calculated by the B3LYP/6-311G(d,p) basis set. We have created the correlation graph in Figure 10 based on the correlation calculations.

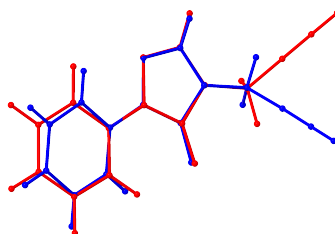


Figure 11. Superimposition diagram of 2PPT [Experimental (X-ray, blue stick model); Theoretical (DFT, red stick model)].

Calculated R^2 values are 0.993 and 0.988 for bond lengths and angles, respectively. According to correlations values, the B3LYP/6-311G(d, p) method gave accurate results for the bond lengths, bond angles, compared with X-ray diffraction studies. The optimized parameters such as bond length and bond angles which are compared with those of experimental values (Table 2).

The second method involves the comparison of the structures obtained with the theoretical calculations by superimposing the molecular skeleton with that obtained from X-ray diffraction giving a RMSE of 3.1 Å for B3LYP/6-311G(d,p) basis sets (Figure 11). According to these results, it may be concluded that the B3LYP/6-311G(d,p) calculation reproduced the geometry of the title compound. Theoretical calculations were carried out in the gas phase while making these comparisons. From the obtained results, it is observed that the B3LYP/6-311G(d,p) calculations very well reproduced the geometry of 2PPT.

4. Conclusions

Interesting developments in electronic devices, geosciences, and pharmaceutical sciences were led by the structural insights from single crystal X-ray diffraction and DFT studies. In addition, knowledge of accurate structural information of active pharmaceutical ingredients (APIs) is a prerequisite for rational drug design. In view of these practical applications, the single crystal X-Ray diffraction, Hirshfeld surface, and DFT based structural analyses of 2PPT is reported. It is interesting to note that the optimized geometrical (DFT) results are found in good conformity with the obtained single X-ray diffraction results (XRD). The Hirshfeld surfaces and fingerprint plots predicted that 2PPT molecule is stabilized by various intermolecular contacts such as C...C, C...H/H...C, H...H, N...C/C...N, N...H, N...N, O...C/O...H, and O...N interactions. MEP predicts the most reactive component in the molecule. Both experimental and theoretical HOMO and LUMO energies determine the charge transfer within the molecule and the difference between HOMO and LUMO energy has supported the chemical and bioactivity properties of 2PPT. E_g of the order of 5.3601 eV indicates the high stability of the 2PPT. B3LYP/6-311G(d,p) calculations very well reproduced the geometry of 2PPT as evidenced by the overlay diagram obtained by X-ray diffraction data.

Acknowledgements

The authors wish to thank the University Science Instrumentation Centre, Karnataka University, Dharwad and Department of Science and Technology - Sophisticated Analytical Instrument Facilities for providing NMR (^1H and ^{13}C NMR) spectra. Shilpa Mallappa Somagond and Ravindra Ramappa Kamble are thankful to University Grants Commission, New Delhi for providing financial assistance under UGC-UPE thrust area "Antitumor activity: An Integrated Approach" [F. No. 14-3/2012(NS/PE) Dated: 14-03-2012] and providing the molecular modelling laboratory facilities.

Supporting information

CCDC-1846037 contains the supplementary crystallographic data for this paper. These data can be obtained free of charge via <https://www.ccdc.cam.ac.uk/structures/>, or by emailing data_request@ccdc.cam.ac.uk, or by contacting The Cambridge Crystallographic Data Centre, 12 Union Road, Cambridge CB2 1EZ, UK; fax: +44(0)1223-336033.

Disclosure statement

Conflict of interest: The authors declare that they have no conflict of interest.

Ethical approval: All ethical guidelines have been adhered.

Sample availability: Samples of the compounds are available from the author.

CRedit authorship contribution statement

Conceptualization: Shilpa Mallappa Somagond; Methodology: Shilpa Mallappa Somagond; Software: Madivalagouda Sannaikar; Validation: Suresh Fakkirappa Madar; Formal Analysis: Jagadeesh Prasad Dasappa; Investigation: Ravindra Ramappa Kamble; Resources: Ravindra Ramappa Kamble; Data Curation: Shankar Madankumar; Writing - Original Draft: Ahmedraza Mavazzan; Writing - Review and Editing: Aravind Raviraj Nesaragi; Visualization: Sanjeev Ramchandra Inamdar; Funding acquisition: Ravindra Ramappa Kamble; Supervision: Ravindra Ramappa Kamble; Project Administration: Ravindra Ramappa Kamble.

ORCID

Shilpa Mallappa Somagond

 <https://orcid.org/0000-0002-0481-3426>

Ahmedraza Mavazzan

 <https://orcid.org/0000-0002-3457-2424>

Suresh Fakkirappa Madar

 <https://orcid.org/0000-0002-4497-2296>

Madivalagouda Sannaikar

 <https://orcid.org/0000-0001-7294-3372>

Shnakar Madan Kumar

 <https://orcid.org/0000-0002-7944-1081>

Sanjeev Ramchandra Inamdar

 <https://orcid.org/0000-0003-3398-4897>

Aravind Raviraj Nesaragi

 <https://orcid.org/0000-0002-6659-2243>

Jagadeesh Prasad Dasappa

 <https://orcid.org/0000-0003-1333-028X>

Ravindra Ramappa Kamble

 <https://orcid.org/0000-0002-0384-655X>

References

- Liu, J.; Liu, Q.; Yang, X.; Xu, S.; Zhang, H.; Bai, R.; Yao, H.; Jiang, J.; Shen, M.; Wu, X.; Xu, J. *Bioorg. Med. Chem.* **2013**, *21* (24), 7742-7751.
- Somagond, S. M.; Kamble, R. R.; Kattimani, P. P.; Joshi, S. D.; Dixit, S. R. *Heterocycl. Comm.* **2017**, *23* (4), 317-324.

- [3]. Chandna, N.; Kapoor, J. K.; Grover, J.; Bairwa, K.; Goyal, V.; Jachak, S. M. *New J. Chem.* **2014**, *38* (8), 3662–3672.
- [4]. Nesaragi, A. R.; Kamble, R. R.; Bayannavar, P. K.; Shaikh, S. K. J.; Hoolageri, S. R.; Kodasi, B.; Joshi, S. D.; Kumbhar, V. M. *Bioorg. Med. Chem. Lett.* **2021**, *41* (127984), 127984.
- [5]. Shaikh, S. K. J.; Sannaikar, M. S.; Kumbhar, M. N.; Bayannavar, P. K.; Kamble, R. R.; Inamdar, S. R.; Joshi, S. D. *ChemistrySelect* **2018**, *3* (16), 4448–4462.
- [6]. Liang, L.; Astruc, D. *Coord. Chem. Rev.* **2011**, *255* (23–24), 2933–2945.
- [7]. Gimadiev, T. R.; Klimchuk, O.; Nugmanov, R. I.; Madzhidov, T. I.; Varnek, A. J. *Mol. Struct.* **2019**, *1198* (126897), 126897.
- [8]. Popov, S. A.; Romanenko, G. V.; Reznikov, V. A. *J. Mol. Struct.* **2008**, *872* (1), 30–39.
- [9]. Naveen; Tittal, R. K.; Ghule, V. D.; Kumar, N.; Kumar, L.; Lal, K.; Kumar, A. *J. Mol. Struct.* **2020**, *1209* (127951), 127951.
- [10]. Larsen, J. S.; Zahran, M. A.; Pedersen, E. B.; Nielsen, C. *Monatsh. Chem.* **1999**, *130* (9), 1167–1173.
- [11]. Cohen, A. J.; Mori-Sánchez, P.; Yang, W. *Chem. Rev.* **2012**, *112* (1), 289–320.
- [12]. Jones, R. O. *Rev. Mod. Phys.* **2015**, *87*, 897–923.
- [13]. Hostaš, J.; Rezáč, J. *J. Chem. Theory Comput.* **2017**, *13* (8), 3575–3585.
- [14]. Kohn, W. *Rev. Mod. Phys.* **1999**, *71* (5), 1253–1266.
- [15]. Bayannavar, P. K.; Sannaikar, M. S.; Madan Kumar, S.; Inamdar, S. R.; Shaikh, S. K. J.; Nesaragi, A. R.; Kamble, R. R. *J. Mol. Struct.* **2019**, *1179*, 809–819.
- [16]. Kattimani, P. P.; Kamble, R. R.; Dorababu, A.; Hunnur, R. K.; Kamble, A. A.; Devarajegowda, H. C. *J. Heterocycl. Chem.* **2017**, *54* (4), 2258–2265.
- [17]. Somagond, S. M.; Wari, M. N.; Shaikh, S. K. J.; Inamdar, S. R.; Shankar, M. K.; Prasad, D. J.; Kamble, R. R. *Eur. J. Chem.* **2019**, *10* (4), 281–294.
- [18]. Sheldrick, G. M. *Acta Crystallogr. A* **2008**, *64* (Pt 1), 112–122.
- [19]. Spek, A. L. *Acta Crystallogr. A* **1990**, *46* (s1), 34–34.
- [20]. Macrae, C. F.; Bruno, I. J.; Chisholm, J. A.; Edgington, P. R.; McCabe, P.; Pidcock, E.; Rodriguez-Monge, L.; Taylor, R.; van de Streek, J.; Wood, P. A. *J. Appl. Crystallogr.* **2008**, *41* (2), 466–470.
- [21]. Domingo, L. R.; Aurell, M. J.; Pérez, P.; Contreras, R. *J. Phys. Chem. A* **2002**, *106* (29), 6871–6875.
- [22]. Lee, C.; Yang, W.; Parr, R. G. *Phys. Rev. B Condens. Matter* **1988**, *37* (2), 785–789.
- [23]. Petersson, G. A.; Al-Laham, M. A. *J. Chem. Phys.* **1991**, *94* (9), 6081–6090.
- [24]. Ditchfield, R. *J. Chem. Phys.* **1972**, *56* (11), 5688–5691.
- [25]. Wolinski, K.; Hinton, J. F.; Pulay, P. *J. Am. Chem. Soc.* **1990**, *112* (23), 8251–8260.
- [26]. Spackman, P. R.; Turner, M. J.; McKinnon, J. J.; Wolff, S. K.; Grimwood, D. J.; Jayatilaka, D.; Spackman, M. A. *J. Appl. Cryst.* **2021**, *54* (3), 1006–1011.
- [27]. Spackman, M. A.; Jayatilaka, D. *CrystEngComm* **2009**, *11* (1), 19–32.
- [28]. Turner, M. J.; McKinnon, J. J.; Jayatilaka, D.; Spackman, M. A. *CrystEngComm* **2011**, *13* (6), 1804–1813.
- [29]. Kumbhar, M. N.; Kamble, R. R.; Dasappa, J. P.; Bayannavar, P. K.; Khamees, H. A.; Mahendra, M.; Joshi, S. D.; Dodamani, S.; Rasal, V. P.; Jalalpure, S. *J. Mol. Struct.* **2018**, *1160*, 63–72.
- [30]. Glusker, J. P.; Lewis, M.; Rossi, M. *Crystal Structure Analysis for Chemists and Biologists*. VCH Publishers New York. 1994, ISBN 0-89573-273-4.
- [31]. Şen, B.; Sevincek, R.; Beksultanova, N.; Dogan, Ö. *J. Mol. Struct.* **2018**, *1173*, 33–41.
- [32]. Panini, P.; Mohan, T. P.; Gangwar, U.; Sankolli, R.; Chopra, D. *CrystEngComm* **2013**, *15* (22), 4549–4564.
- [33]. Sathish, M.; Meenakshi, G.; Xavier, S.; Sebastian, S.; Periandy, S.; Ahmad, N.; Jamalis, J.; Rosli, M.; Fun, H.-K. *J. Mol. Struct.* **2018**, *1164*, 420–437.
- [34]. McKinnon, J. J.; Jayatilaka, D.; Spackman, M. A. *Chem. Commun. (Camb.)* **2007**, No. 37, 3814–3816.
- [35]. Spackman, M. A.; McKinnon, J. J. *CrystEngComm* **2002**, *4* (66), 378–392.
- [36]. Singh, R. N.; Kumar, A.; Tiwari, R. K.; Rawat, P. *Spectrochim. Acta A Mol. Biomol. Spectrosc.* **2013**, *113*, 378–385.
- [37]. Sjöberg, P.; Politzer, P. *J. Phys. Chem.* **1990**, *94* (10), 3959–3961.
- [38]. Lee, B.; Richards, F. M. *J. Mol. Biol.* **1971**, *55* (3), 379–400.
- [39]. Weiner, P. K.; Langridge, R.; Blaney, J. M.; Schaefer, R.; Kollman, P. A. *Proc. Natl. Acad. Sci. U. S. A.* **1982**, *79* (12), 3754–3758.
- [40]. Connolly, M. L. *Science* **1983**, *221* (4612), 709–713.
- [41]. Francl, M. M.; Hout, R. F., Jr; Hehre, W. J. *J. Am. Chem. Soc.* **1984**, *106* (3), 563–570.
- [42]. Artica, G. A.; Jammal, V. B.; Mezey, P. G.; Yadav, J. S.; Hermsmeier, M. A.; Gund, T. M. *J. Mol. Graph.* **1988**, *6* (1), 45–53.
- [43]. Dunitz, J. D.; Filippini, G.; Gavezzotti, A. *Tetrahedron* **2000**, *56* (36), 6595–6601.
- [44]. Bondi, A. Van Der Waals Volumes and Radii. *J. Phys. Chem.* **1964**, *68* (3), 441–451.
- [45]. Vasanthakumari, R.; Nirmala, W.; Sagadevan, S.; Mugeshini, S.; Rajeswari, N.; Balu, R.; Santhakumari, R. *J. Mol. Struct.* **2021**, *1239* (130449), 130449.
- [46]. Naresh, P.; Pramodh, B.; Naveen, S.; Ganguly, S.; Panda, J.; Sunitha, K.; Maniukiewicz, W.; Lokanath, N. K. *J. Mol. Struct.* **2021**, *1236* (130228), 130228.



Copyright © 2021 by Authors. This work is published and licensed by Atlanta Publishing House LLC, Atlanta, GA, USA. The full terms of this license are available at <http://www.eurjchem.com/index.php/eurjchem/pages/view/terms> and incorporate the Creative Commons Attribution-Non Commercial (CC BY NC) (International, v4.0) License (<http://creativecommons.org/licenses/by-nc/4.0>). By accessing the work, you hereby accept the Terms. This is an open access article distributed under the terms and conditions of the CC BY NC License, which permits unrestricted non-commercial use, distribution, and reproduction in any medium, provided the original work is properly cited without any further permission from Atlanta Publishing House LLC (European Journal of Chemistry). No use, distribution or reproduction is permitted which does not comply with these terms. Permissions for commercial use of this work beyond the scope of the License (<http://www.eurjchem.com/index.php/eurjchem/pages/view/terms>) are administered by Atlanta Publishing House LLC (European Journal of Chemistry).